Bioorganic & Medicinal Chemistry 18 (2010) 7900–7910

Contents lists available at ScienceDirect

Bioorganic & Medicinal Chemistry

journal homepage: www.elsevier.com/locate/bmc

Identification by high-throughput screening of inhibitors of *Schistosoma mansoni* NAD$^+$ catabolizing enzyme

Isabelle Kuhn [a], Esther Kellenberger [b], Fatouma Said-Hassane [a], Pascal Villa [c], Didier Rognan [b], Annelise Lobstein [b], Jacques Haiech [b,c], Marcel Hibert [b], Francis Schuber [a], Hélène Muller-Steffner [a,*]

[a] *Laboratoire de Conception et Application de Molécules Bioactives, UMR 7199 CNRS, Université de Strasbourg, Faculté de Pharmacie, 74 route du Rhin, 67400 Illkirch, France*
[b] *Laboratoire d'Innovation Thérapeutique, UMR 7200 CNRS, Université de Strasbourg, Faculté de Pharmacie, 67400 Illkirch, France*
[c] *PCBIS, UMS 3286 CNRS, Université de Strasbourg, ESBS and Faculté de Pharmacie, 67412 Illkirch, France*

ARTICLE INFO

Article history:
Received 11 June 2010
Revised 14 September 2010
Accepted 16 September 2010
Available online 25 September 2010

Keywords:
Schistosoma mansoni
*Sm*NACE
CD38
High-throughput screening
Fluorescence
Flavonoids
Anthocyanidins
Docking

ABSTRACT

Schistosomiasis is a major tropical parasitic disease. For its treatment, praziquantel remains the only effective drug available and the dependence on this sole chemotherapy emphasizes the urgent need for new drugs to control this neglected disease. In this context, the newly characterized *Schistosoma mansoni* NAD$^+$ catabolizing enzyme (*Sm*NACE) represents a potentially attractive drug target. This potent NAD$^+$glycohydrolase, which is localized to the outer surface (tegument) of the adult parasite, is presumably involved in the parasite survival by manipulating the host's immune regulatory pathways. In an effort to identify *Sm*NACE inhibitors, we have developed a sensitive and robust fluorometric high-throughput screening assay. The implementation of this assay to the screening of a highly diverse academic chemical library of 14,300 molecules yielded, after secondary assays and generation of dose–response curves, the identification of two natural product inhibitors, cyanidin and delphinidin. These confirmed hits inhibit *Sm*NACE with IC_{50} values in the low micromolar range. To rationalize the structure–activity relationship, several related flavonoids were tested, thereby leading to the identification of 15 additional natural product inhibitors. A selection of representative flavonoid inhibitors indicated that although they also inhibit the homologous human CD38, a selectivity in favor of *Sm*NACE could be reached. Docking studies indicated that these inhibitors mimic the binding mode of the enzyme substrate NAD$^+$ and suggested the pharmacophoric features required for *Sm*NACE active site recognition.

1. Introduction

Schistosomiasis is a major parasitic disease which affects over 200 million individuals worldwide. It is endemic in 74 countries in (sub)tropical regions of Africa, Asia and South America. Despite considerable efforts over the past decades, no protective vaccine is yet in sight. Only one efficient and safe drug is currently available, namely praziquantel.[1] The development of resistance raises concerns about the urgent need for alternative drugs to control, in the long-term, this 'neglected' tropical disease.

Schistosomes, like the other parasitic helminths, are known for their ability to survive within their hosts for extended time periods. This has been ascribed to their capability to manipulate the host immune regulatory pathways. Thus, the parasites establish a chronic inflammation and polarize the immune response towards a strong and contained immunosuppressive CD4$^+$ Th2 cell response.[2] Another survival strategy of the pathogen during a chronic infection involves the induction of immunosuppressive regulatory T-lymphocytes (Tregs).[3] Although much progress has been made recently, understanding of the molecular basis underlining the mechanisms which allow the parasite to subvert the host immune system remains limited.

We have recently characterized in the platyhelminth *Schistosoma mansoni* a NAD$^+$ catabolizing enzyme (*Sm*NACE) whose expression is developmentally regulated.[4] *Sm*NACE is a GPI-anchored protein localized to the outer tegument of the adult parasite. The high levels of this efficient NAD$^+$glycohydrolase at the surface of adult schistosomes can impact on NAD$^+$-dependent pathways of the human immune system, most probably by scavenging the host's extracellular/circulating free NAD$^+$. The two main processes which can be affected are: (i) NAD$^+$-induced apoptosis of naïve T-lymphocyte sub-populations, including Tregs, via cell-surface ADP-ribosyltransferases catalyzed ADP-ribosylation reactions,[5] and (ii) the formation of cyclic ADP-ribose, a Ca^{2+}-mobilizing messenger, produced from NAD$^+$ by ecto-CD38,[6] which is involved in many cellular pathways including chemotactism of neutrophils

Abbreviations: *Sm*NACE, *Schistosoma mansoni* NAD$^+$ catabolizing enzyme; ε-NAD$^+$, 1,N^6-etheno NAD$^+$; HTS, high-throughput screening; PARP, poly(ADP-ribose) polymerase; GPI, glycosylphosphatidylinositol.

* Corresponding author. Tel.: +33 368 85 41 69; fax: +33 368 85 43 06.
E-mail address: steffner@bioorga.u-strasbg.fr (H. Muller-Steffner).

0968-0896/$ - see front matter © 2010 Elsevier Ltd. All rights reserved.
doi:10.1016/j.bmc.2010.09.041

and dendritic cells.[7] In the context of drug discovery, *Sm*NACE represents therefore a new attractive target, because of its extra-cellular location and its potential role in the pathogen interference with the host immunity.

The present work aimed at the identification of *Sm*NACE inhibitors, which will next serve as pharmacological tools for in vivo functional studies and target validation. Since *Sm*NACE is a distant homolog to mammalian CD38 a good starting point would have been to test known CD38 inhibitors. However, considering the paucity of existing druggable small-molecule inhibitors of CD38, it was highly desirable to search for new leads. To that end we have developed an efficient and reliable high-throughput screening assay for the identification of *Sm*NACE inhibitors. We screened 14,300 molecules of the French academic compound library and identified two anthocyanidins, cyanidin and delphinidin, able to inhibit *Sm*NACE in vitro, with IC_{50} values in the low micromolar range. Structure–activity relationship analyses were performed with structurally related flavonoids, thereby leading to the identification of additional inhibitory natural products. The interactions between these compounds and the active site of the target enzyme were suggested by docking studies. They provided insights into the possible structural features required for the inhibition of *Sm*NACE by this novel class of inhibitors.

2. Results

*Sm*NACE, a member of the ADP-ribosyl cyclase super-family, is closely related to the mammalian CD38.[4] However, the inhibitors of CD38 available today are mainly dyes such as Cibacron blue 3GA,[8] mechanism-based inhibitors like 2′deoxy-2′-fluoroarabino-NMN^+,[9] and non-hydrolyzable analogs of NAD^+.[10] Unfortunately, all these molecules are inadequate templates for drug design, moreover some of them are much less efficient against *Sm*NACE than against human CD38.[8] Considering the paucity of existing small-molecule inhibitors of *Sm*NACE, it was highly desirable to search for new compounds. We first investigated some schistosomicidal drugs and representative inhibitors of NAD^+-utilizing enzymes, such as the much studied NAD^+-dependent sirtuins[11] and poly(ADP-ribose) polymerases.[12] Because of the mitigated results, we have finally developed a convenient fluometric assay for the high-throughput screening of French academic chemical libraries (14,300 molecules).

2.1. Selected schistosomicidal drugs do not target *Sm*NACE

The mode of action of praziquantel (Fig. 1), the only currently available efficient anti-schistosomal drug, is still debated.[1] However accumulated evidence points to a disruption of Ca^{2+} homeostasis within the parasites, involving for example, increased fluxes through voltage-gated Ca^{2+} channels. Given the homology of *Sm*NACE to ecto-enzymes involved in the production Ca^{2+}-mobilizing metabolites like cyclic ADP-ribose and $NAADP^+$,[4] this enzyme was a potential target. When tested with a fluorometric assay using 1,N^6-etheno NAD^+ as substrate, at concentrations up to 100 μM praziquantel did not inhibit *Sm*NACE.

Curcumin (Fig. 1), the major constituent of *Curcuma longa*, has many therapeutic applications including its much investigated anticancer activity.[13] However, this natural product was recently also demonstrated to have an efficient in vitro schistosomicidal activity at low micromolar concentrations.[14] Similarly, the known antimalarial drugs chloroquine and mefloquine, were also shown to be active against schistosomes in vivo.[15] These three compounds did not inhibit (fluorometric assay) *Sm*NACE up to100 μM.

2.2. Selected NAD^+-utilizing enzymes inhibitors do not inhibit *Sm*NACE

NAD^+ serves as substrate for a large number of enzymes, which share with *Sm*NACE and CD38 common mechanistic features, that is, recognition of NAD^+ and catalysis of the cleavage of its ribosyl-nicotinamide bond. Among these enzymes are mono-ADP-ribosyltransferases and two other categories, NAD^+-dependent protein deacylases (sirtuins) and PARPs, which have generated a tremendous interest, including for the design and development of drugs. We have tested on *Sm*NACE representative inhibitors of these enzymes.

PJ-34 (Fig. 1) is a potent water-soluble competitive inhibitor which is bound within the nicotinamide-binding pocket of the catalytic domain of *Pseudomonas aeruginosa* exotoxin A[16] a mono-ADP-ribosyltransferase, and of poly(ADP-ribose) polymerase-3.[17] Suramin (Fig. 1) was identified as a potent and selective inhibitor of sirtuins SIRT-1, -2 and -5.[18] Interestingly this compound, with its aromatic rings and numerous sulfonate substituents, shares some structural features with Cibacron Blue 3GA, a known inhibitor of CD38 and, to a lesser extent, of *Sm*NACE. Finally, 1,8-naphthalimide (NAP) (Fig. 1) was also demonstrated to be a potent in vitro inhibitor of the mono-ADP-ribosyltransferase activity of bacterial toxins.[19] When tested at concentrations up to 100 μM with the fluorometric assay, all these compounds failed to inhibit significantly *Sm*NACE (less than 10% at 100 μM).

2.3. Design of a high-throughput screening assay

High-throughput screening was considered to be an alternative strategy for the identification of small-molecule inhibitors of *Sm*NACE. This implied to design a robust and sensitive assay that could be performed in a multi-well plate format. Such a high-throughput fluorescence-based assay, based on a specific cyclic ADP-ribose detection, was previously developed for related enzymes such as ADP-ribosyl cyclase and CD38.[20] However, this method cannot be extended to *Sm*NACE because of the incapacity of this enzyme to transform NAD^+ into cyclic ADP-ribose.[8] Moreover the routine fluorometric method using 1,N^6-etheno NAD^+ as substrate[21] proved also to be inappropriate as the product detection wavelength at 410 nm corresponds to a range in which many library compounds absorb light, thus leading to spectral interference and false-positives.

We therefore developed an assay based on a known highly sensitive fluorometric quantification of the alkylpyridinium moiety of NAD^+. It involves a chemical reaction, under basic conditions, of the residual substrate with ketones, such as acetophenone,[22] yielding a fluorescent compound with a fluorescence signal emitted at 460 nm (λ_{ex} = 355 nm) which is suitable for an HTS assay (Fig. S1). This method, which has been used previously with other NAD^+-dependent enzymes,[23,24] can be easily miniaturized, automated and applied to a 96-well plate format for HTS.

Screening of enzyme inhibitors with a single end-point assay, such as the one used in this work, requires an optimization of several parameters among which reaction progress is of paramount importance to achieve a good sensitivity. Related to that point, it was shown previously that measurement of the signal at high substrate conversion levels maximizes the detection of inhibitors without compromising the value of the apparent IC_{50}.[25] Consequently in our standard HTS conditions, NAD^+ concentration was set at 10 μM, that is, $[S]/K_m = 0.26$, and the concentration of *Sm*NACE and reaction times were adjusted to reach 60–70% reaction progress. In addition the following controls were performed: (i) the tolerance to DMSO was determined and no significant decrease in enzyme activity was observed up to 0.1% (v/v); (ii) to

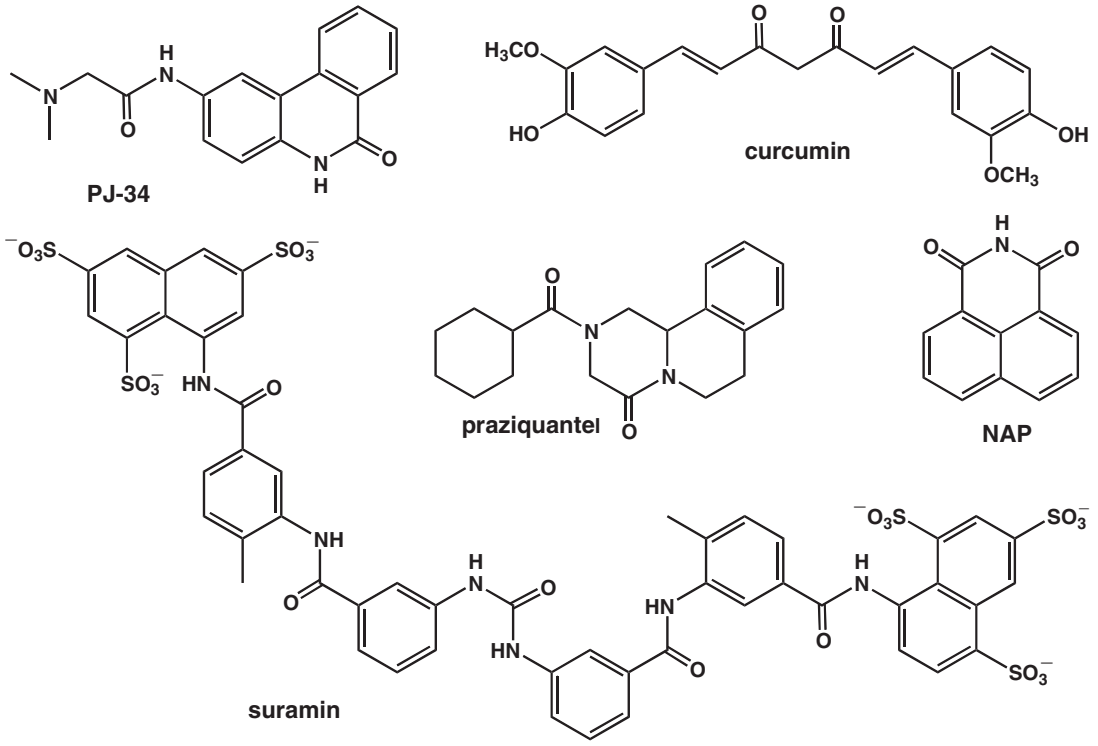

Figure 1. Structure of molecules tested against *Sm*NACE.

assess the performance of the assay, three wells/plate containing 100 μM of the *Sm*NACE inhibitor Cibacron Blue 3GA (IC_{50} = 1.15 ± 1.14 μM)[8] were used as positive controls; (iii) ADP-ribose generated by the reaction did not interfere with the enzyme activity, that is, no product inhibition was observed, nor with the fluorescence signal. The quality of the assay was validated by the average value found for the Z' factor = 0.72 ± 0.12 which is considered an excellent assay[26] in which a large signal/background ratio is observed (Z' values were determined in all screening plates as they all contained the controls).

2.4. High-throughput screening results

A French academic compound library (total of 14,300 molecules) characterized by an important chemical diversity[27] with potential pharmacologic activities was screened for inhibitors of *Sm*NACE using the HTS assay described above. With a threshold of 40% inhibition at 10 μM, 145 hits were obtained. The compounds presenting an intrinsic fluorescence were eliminated (29 compounds). Hit confirmation was performed in duplicate at 1 μM and 10 μM on the 116 primary hits. We could confirm the inhibition >40% for 53 of the compounds (46%). Among them 11 showed an inhibition over 40% when tested at 1 μM. These ones were selected to be validated and inhibition of *Sm*NACE was investigated in greater detail by performing individual assays with compounds which originated from the original compound stock and/or obtained commercially (anthocyanidins) in an analytically pure form. Dose–response curves were established fluorometrically using the microplate assay described above and/or by kinetic measurements using ε-NAD^+ as substrate. Colloidal aggregation leading to promiscuous inhibition of enzymes is well recognized as a source of false-positives.[28] This irrelevant inhibition being abolished in the presence of detergent, assays were also conducted in the presence of 0.1% Triton X-100. After eliminating the false-positives and the non-reproducible hits inherent to the HTS approach we finally identified two anthocyanidins, cyanidin (**1**) and delphinidin (**2**) that are able to inhibit *Sm*NACE with IC_{50} values in the low micromolar range (Fig. 2). For cyanidin, the best inhibitor, the IC_{50} was 2.3 ± 0.1 μM (Table 1). Importantly the slope of the dose–response curve (Hill coefficient) was found equal to −1, a result expected for a classical single-site inhibition by this natural product as opposed to steeper slopes triggered for example, artifactually by colloidal aggregators.[28] Additional experiments were performed which demonstrated that cyanidin is a competitive inhibitor of *Sm*NACE with respect to the substrate with a K_i = 2.1 ± 0.4 μM) (Fig. S2). Delphinidin is structurally very similar to cyanidin and, with an IC_{50} of 6.0 μM, this anthocyanidin is a little less potent.

2.5. Structure–activity relationship study

Our HTS campaign yielded two confirmed hits, namely cyanidin and delphinidin. Both belong to the anthocyanidin family of flavonoids. These compounds consist in flavylium cations, that is, a six-membered aromatic ring (ring A) *ortho*-fused to a pyrylium ring (ring C), namely the benzopyrylium, linked at the 2-position to a phenyl group (ring B). In anthocyanidins, the flavylium cation can carry hydroxyl and/or hydroxymethyl substituents at positions 3, 5, 6 and 7 of the benzopyrylium moiety, and at position 3′, 4′ and 5′ of ring B (Fig. 2).

To delineate which structural determinants in cyanidin (**1**) and delphinidin (**2**) are important for their interaction with the active site of *Sm*NACE, we tested the potency of structurally related commercially available flavonoids (compounds **3**–**18**, Figs. 3 and 4) and *trans*-stilbenoids **19, 20** (Fig. 4). The structure–activity relationship study mainly focus on: (i) the number and the position of hydroxyl groups, and the effect of their methylation or glycosylation, and (ii) the importance of the flavylium cation whose charge could mimic the oxocarbenium ion-like transition state occurring during the reaction pathway of CD38/*Sm*NACE-catalyzed cleavage of the ribo-

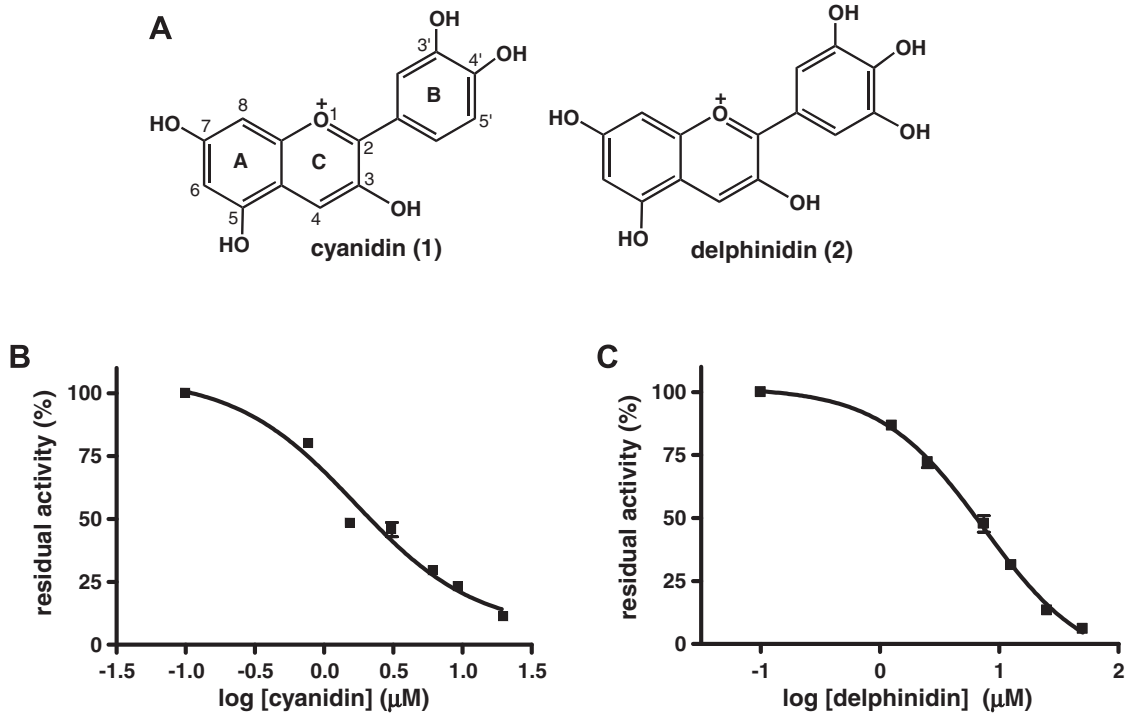

Figure 2. Structure of cyanidin (**1**) and delphinidin (**2**)—Concentration-dependent inhibition of recombinant *Sm*NACE by cyanidin. (A) Conventional numbering in anthocyanidins is displayed on the cyanidin (**1**) structure. (B and C) Residual enzyme activity, in percent, determined fluorometrically using 1,N^6-etheno NAD$^+$ as substrate, is plotted as a function of the log of inhibitor concentration and analyzed by non-linear regression.

Table 1
IC_{50} values for the inhibition of *Sm*NACE by natural products identified by HTS and SAR studies

No.	Compound	IC_{50}[a] (μM)
1	Cyanidin	2.3 ± 0.1
2	Delphinidin	6.0 ± 0.3
3	Quercetagetinidin	6.1 ± 0.3
4	Pelargonidin	4.4 ± 0.4
5	Luteolinidin	5.9 ± 0.2
6	Fisetinidin	6.4 ± 0.6
7	Peonidin	5.6 ± 0.7
8	Petunidin	37.8 ± 1.14
9	Malvidin	8.0 ± 1.4
10	Diosmetinidin	9.9 ± 0.4
11	Kuromanin	8.2 ± 0.8
12	Quercetin	3.9 ± 0.4
13	Myricetin	22.0 ± 1.3
14	Robinetin	5.8 ± 0.7
15	Quercetagetin	1.3 ± 0.2
16	Luteolin	8.4 ± 0.4
17	*rac*-Taxifolin	19.5 ± 1.4
18	*rac*-Catechin	>100[b]
19	Piceatannol	>100[b]
20	*trans*-Resveratrol	>100[b]

[a] Determined fluorometrically using 1,N^6-etheno NAD$^+$ as substrate. The values represent means ± SD of three independent experiments.
[b] No inhibition was detectable at 100 μM.

syl-nicotinamide bond of the substrate NAD$^+$.[29] The IC_{50} values reported in Table 1 were obtained with the fluorometric assay, using 1,N^6-etheno NAD$^+$ as substrate; importantly they were all validated by an independent HPLC assay using NAD$^+$ as substrate (see Section 4.3).

The relative importance of the hydroxyl substituents was studied by testing eight additional anthocyanidins (**3**–**10**) and one anthocyanin (**11**) which were compared to **1** and **2**. Comparatively to cyanidin (**1**), which contains five hydroxyl substituents, at position 3, 5 and 7 of the benzopyrylium moiety and at position 3′ and 4′ of ring B, delphinidin (**2**) carries an additional hydroxyl substituent at position 5′ resulting in about a 2–3-fold lesser potency (see above; Table 1). Quercetagetinidin (**3**) also differs from cyanidin by a single additional hydroxyl substituent, here at position 6 of ring A. With an IC_{50} of 6.1 μM (Table 1), it is as potent as delphinidin. Pelargonidin (**4**) only carries four hydroxyl substituents and lacks the 3′-OH of cyanidin ring B. It efficiently inhibits *Sm*NACE activity, with a potency intermediate between that of cyanidin and delphinidin. Like pelargonidin, luteolinidin (**5**) and fisetinindin (**6**) only carry four hydroxyl substituents, and respectively lack the 3-OH and the 5-OH of the cyanidin benzopyrilium moiety. These two anthocyanidins have both IC_{50} values close to 6 μM. In summary, the inhibitory potency of cyanidin is decreased 2–3-fold if one of its hydroxyl groups at position 3, 5 or 3′ is absent, or if an extra hydroxyl group at positions 6 or 5′ is added. Next, four methylated derivatives of anthocyanidins (**7**–**10**) were tested for their capacity to inhibit *Sm*NACE. Peonidin (**7**), petunidin (**8**), malvidin (**9**) and diosmetinidin (**10**) are respectively monomethylated cyanidin and delphinidin, dimethylated delphinidin and monomethylated luteolinidin (Fig. 3). All four compounds inhibit the enzyme, but the observed IC_{50} values ranging from 5.6 to 37.8 μM, are 1.3 to 6.3-fold higher than the IC_{50} of their non-methylated parent anthocyanidins. Finally, we tested an anthocyanin, namely kuromanin (**11**). Kuromanin inhibits *Sm*NACE with an IC_{50} of 8.2 μM. Thus, glycosylation of cyanidin at position-3 yields a 3.5-fold decrease of its inhibitory potency. In conclusion, all tested anthocyanidins inhibit *Sm*NACE at low micromolar concentrations, and the optimal substitution pattern of the flavylium cation is found in cyanidin (**1**).

The importance of the flavylium ion was investigated by use of analogs modified in ring C. We have tested four members of the flavonol subgroup (**12**–**15**) and one flavone (**16**) which lacks the 3-OH group. Their common scaffold is 2-phenyl-1,4-benzopyrone, characterized by the presence of a keto group at position 4 of ring C and by the occurrence of a neutral form of the oxygen at position-1 of ring C. Quercetin (**12**), myricetin (**13**), quercetagetin

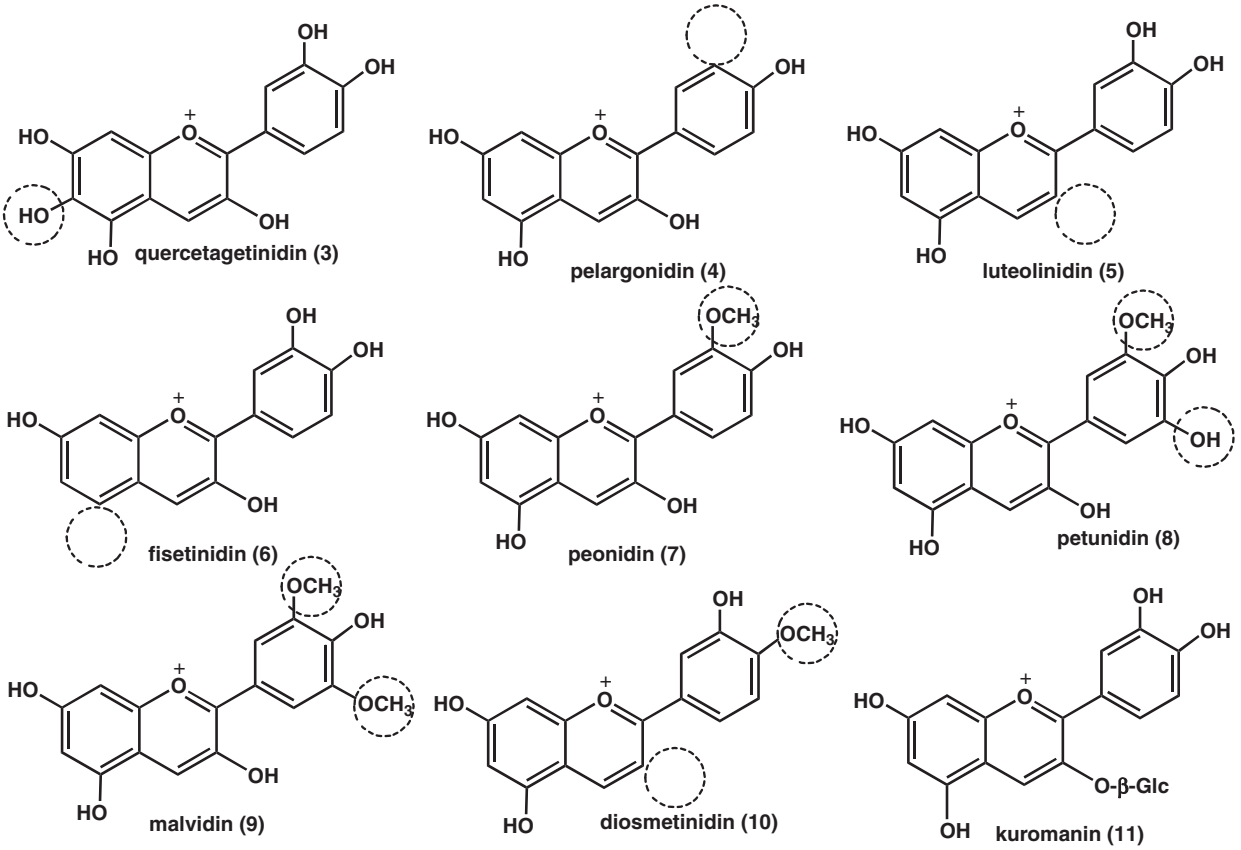

Figure 3. Anthocyanidins tested as inhibitors of *Sm*NACE. Dotted-circles highlight the modifications with respect to the structure of cyanidin.

(**15**) and luteonin (**16**) have the same hydroxyl substitution patterns than cyanidin, delphinidin, quercetagetinidin and luteolinidin, respectively. Whereas quercetin, myricetin and luteonin are 2–4 times less potent than their anthocyanidin counterparts, quercetagetin is seemingly the most potent inhibitor of *Sm*NACE activity with an IC_{50} of 1.3 μM. Robinetin (**14**) is a flavonol closely related to myricetin, which only lacks its hydroxyl group at position 5. The inhibitory potency of **14** is about four times higher than that of myricetin.

Next we tested the flavanonol taxifolin (**17**), that is, a 2,3-dihydroflavone, which differs from quercetin by the reduction of the C2–C3 double bond and the consequent distortion of ring C plane. Taxifolin inhibits *Sm*NACE at low micromolar concentrations, but is five times less potent than quercetin. To further investigate the importance of ring C planarity, we then tested catechin (**18**), which is a flavan-3-ol. Catechin is a close analog of taxifolin, but lacks the keto group at position 4 of ring C. **18** displayed no inhibition of *Sm*NACE at 100 μM, suggesting that the three-dimensional shape of the flavone scaffold better suits the enzyme active site than the flavane one.

Finally we also tested two *trans*-stilbenoids, piceatannol (**19**) and resveratrol (**20**), which are structurally related to anthocyanidins yet do not include ring C. Neither compound inhibits *Sm*NACE at 100 μM.

Altogether the SAR study allowed the discovery of 15 additional micromolar inhibitors of *Sm*NACE. All inhibitors belong to the flavonoid family of plant metabolites. With an IC_{50} of 1.3 μM quercetagetin (**15**) is the most potent inhibitor of this series of compounds. In addition, we identified key structural features for *Sm*NACE inhibition: (i) the nature of ring C, which impacts its geometry and reactivity, (ii) the substitution of free hydroxyl groups in rings A, B and C (see Section 3).

2.6. Modeling of *Sm*NACE active site

To further gain insight into the structural determinants of the enzyme inhibition, the three-dimensional structure of *Sm*NACE has been modeled by homology to human CD38.[8] Its active site was compared to the 7070 sites of sc-PDB,[30] which is a collection of all druggable binding sites available in the PDB. The sc-PDB contains 2377 different proteins, including 144 different NAD^+-binding proteins. It also contains three targets of PJ-34 (a viral mono-ADP-ribosyltransferase, the catalytic domain of *P. aeruginosa* exotoxin A and PARP-1), and potential targets of suramin (human histone deacetylases subtype-4, -6 and -8, and a bacterial histone deacetylase-like protein). Each sc-PDB site was 3D-aligned to the active site of *Sm*NACE, and three scores were computed to evaluate the structural similarity. Using empirical distance thresholds for discriminating similar from dissimilar ligand-binding sites[31] we retained only two hits: the *Sm*NACE binding site was only found similar to human CD38 and to its homolog BST1/CD157, and not to any other NAD^+-binding protein including the known targets of PJ-34 or suramin. This important observation suggests that the recognition of NAD^+ by *Sm*NACE, and by the members of the CD38 family, involves specific structural features which are not shared by any other enzyme families utilizing NAD^+.

2.7. Docking of flavonoids to the active site of *Sm*NACE

All the inhibitors were individually docked into the binding site of *Sm*NACE, using two different programs (GOLD and SURFLEX). The modeled three-dimensional complexes have high docking scores, no intermolecular bumps and no internal distortions of the ligand (Table S1). The predicted binding modes consistently suggest that flavonoids can mimic the nicotinamide-ribosyl moiety of the

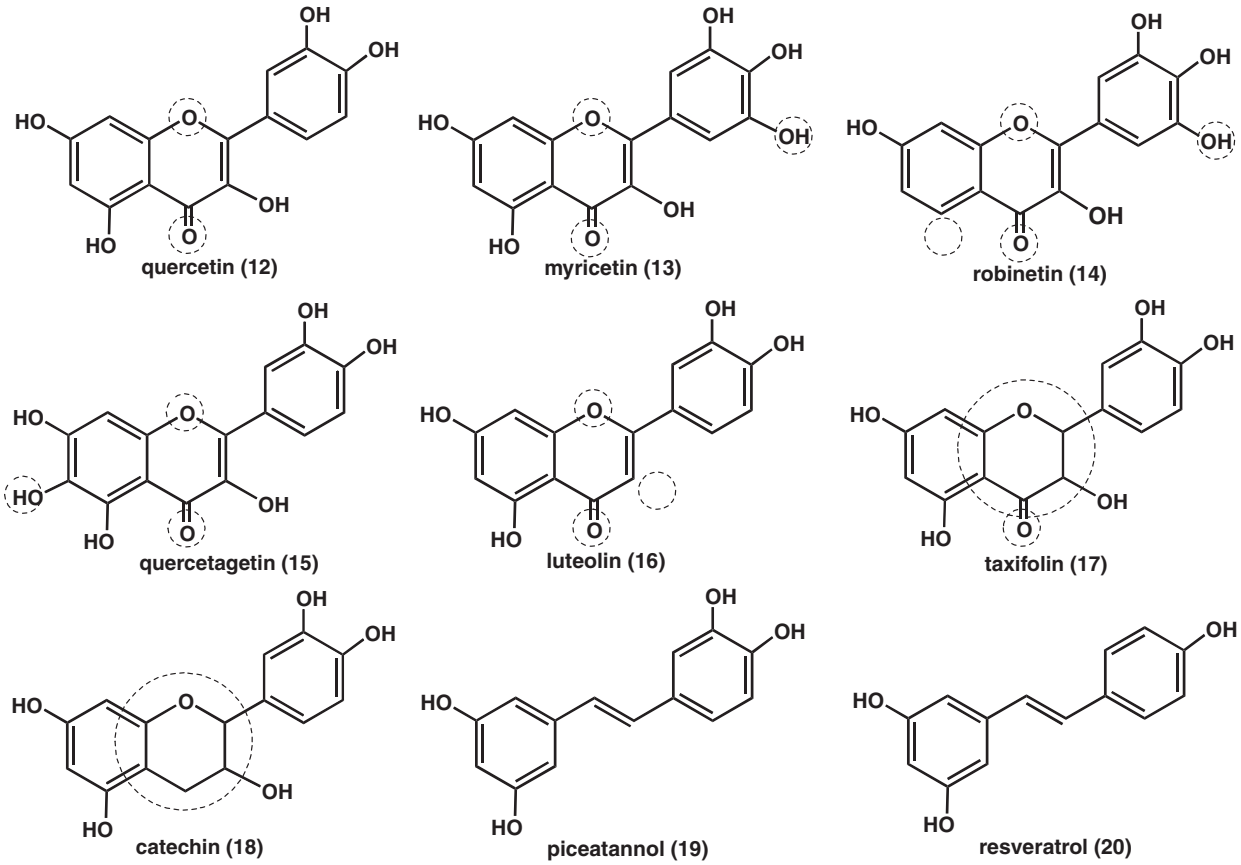

Figure 4. Flavonoids tested as inhibitors of *Sm*NACE. Dotted-circles indicate the modifications with respect to the structure of cyanidin. Compounds **12**–**15** are flavonols; compound **16** is a flavone; compound **17** is a flavanonol and **18** a flavan-3-ol. Compounds **19** and **20** are *trans*-stilbenoids.

substrate NAD^+. In the crystal structure of NAD^+ in complex with human CD38 (Fig. 5A),[32] the NAD^+ pyridinium is stacked against the conserved residue Trp189 (cation–π interaction). The orientation of NAD^+ nicotinamide in the active site is fixed by two hydrogen bonds established between the nitrogen atom of its amide group and the side-chains of Glu146 and Glu155. The position of the NAD^+ nicotinamide induces the placement of NAD^+ ribose in the bottom of the protein pocket. The NAD^+ ribose establishes efficient H-bonds to the catalytic residue Glu226 (which is mutated into a Glutamine in Fig. 5A), and to a buried crystal water molecule. Fig. 5B–D shows the *Sm*NACE-bound modeled structures of cyanidin, taxifolin and quercetagetin, which are the best inhibitors of the flavonoids subgroups studied here. In the three modeled complexes, the flavonoid phenyl ring B fills the ribose-binding subsite, and can H-bond to a buried water molecule, to His103 backbone NH-group and to Glu202 carboxylate. Glu202 was demonstrated by site-directed mutagenesis to be the catalytic residue of the enzyme (I. Kuhn et al., to be published). The flavonoid rings A and C fill the nicotinamide-binding subsite, and are stacked against the conserved residue Trp165, with putative H-bonds to Glu124 carboxylate, Asp133 carboxylate and to Thr197 hydroxyl and/or His162 imidazole.

Whatever the studied flavonoid, docking did not yield a single pose of the molecule into *Sm*NACE active site, but rather a homogeneous ensemble of distinct poses (Figs. S3–S5). In all generated poses, the flavonoid and NAD^+ nicotinamide-ribosyl coincide, with systematic H-bonding to the catalytic Glu and to the nearby buried water molecule. The poses vary in their total H-bond networks, which also involve two to four of the protein polar residues His103, Glu124, Asp133, His162 and Thr197. Last, in a few models (Fig. S5), the flavonoid phenyl ring B fills the nicotinamide-binding subsite whereas rings A and C fill the ribose-binding subsite. In this binding mode too, the catalytic Glu202 is the key anchoring residue. In favor of this assumption we have recently obtained preliminary data (I. Kuhn et al.) indicating that, compared to wild-type *Sm*NACE, the IC_{50} value for cyanidin was increased by more than 2-orders of magnitude with the Glu202Ala mutant.

The docking study clearly indicates that flavonoids are structural analogs of nicotinamide ribonucleoside, sharing similar binding mode to key residues of *Sm*NACE catalytic site. The three-dimensional models are consistent with the structure–activity data. Hence, the variations in the substitution pattern of anthocyanidins **1**–**11** do not alter the directional interactions with *Sm*NACE (H-bond to Glu202, and to at least two other polar residues). Last, the overall three-dimensional shapes of the flavonoids **12**–**17** and their corresponding anthocyanidins are comparable, therefore they most probably share similar binding mode to *Sm*NACE.

2.8. Selectivity of the flavonoid inhibitors: *Sm*NACE versus human CD38

*Sm*NACE represents a novel potential target to fight schistosomiasis. It shares with CD38 of the human host structural and functional similarities. The discovery of the flavonoids which inhibit *Sm*NACE in the low micromolar range prompted us to evaluate their selectivity against human CD38. As shown in Table 2, the study of a selection of representative members of the different flavonoid subgroups studied in this work, revealed that these molecules are also effective against CD38. However two of these inhibitors, cyanidin (**1**) and quercetin (**12**), show a selectivity of

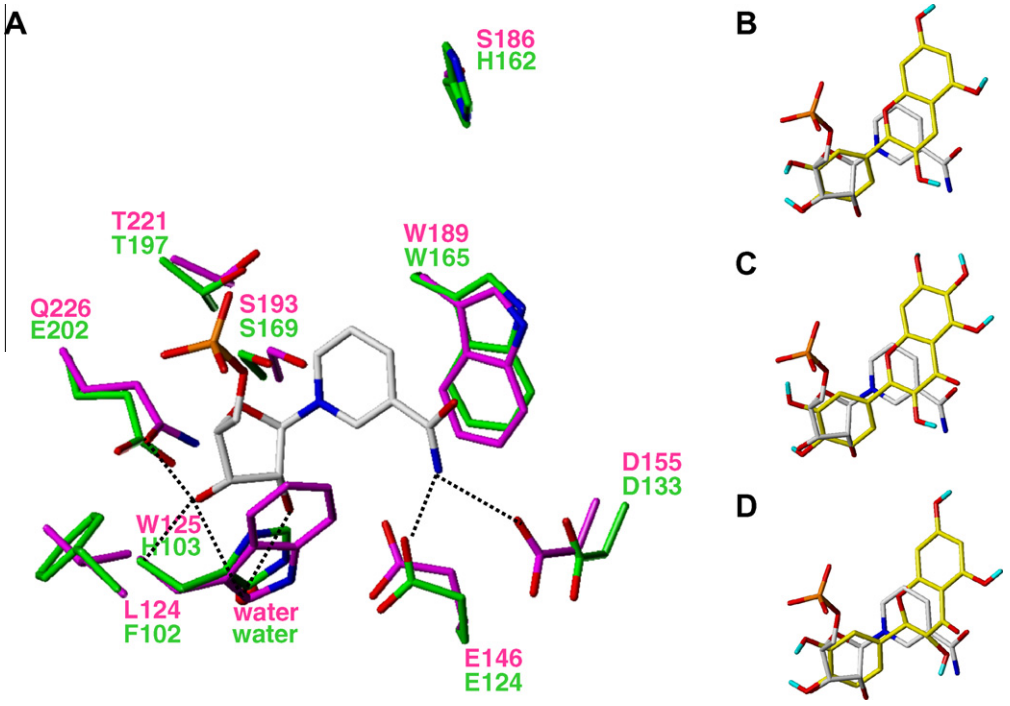

Figure 5. Three-dimensional structure of *Sm*NACE/CD38 active sites in complex with substrate/competitive inhibitor flavonoids. For sake of clarity only the NMN^+ moiety of NAD^+ is displayed. All molecules are shown as capped sticks. Color coding: oxygen, red; nitrogen, blue; hydrogen, cyan (only polar hydrogen atoms are represented); carbon, grey, yellow, green and magenta for NAD^+, flavonoid, *Sm*NACE and CD38, respectively. (A) Crystal structure of NAD^+ bound to human CD38 E226Q mutant (PDB code 2i65). The three-dimensional model of *Sm*NACE is superimposed to the crystal structure of human CD38. The protein binding sites are represented by the side-chains of key active site residues. (B) 3D-model of *Sm*NACE-bound cyanidin, superimposed to the crystal structure of CD38-bound NAD^+. (C) 3D-model of *Sm*NACE-bound quercetagetin, superimposed to the crystal structure of CD38-bound NAD^+. (D) 3D-model of *Sm*NACE-bound taxifolin, superimposed to the crystal structure of CD38-bound NAD^+.

Table 2
Comparative IC_{50} values for the inhibition of *Sm*NACE and human CD38

No.	Compound	IC_{50}^{SmNACE}[a] (μM)	IC_{50}^{CD38}[a] (μM)	Selectivity for *Sm*NACE[b]
1	Cyanidin	2.3 ± 0.1	21.8 ± 2.6	9.5
8	Pelargonidin	4.4 ± 0.4	16.3 ± 2.0	3.7
11	Kuromanin	8.2 ± 0.8	6.3 ± 0.6	0.8
12	Quercetin	3.9 ± 0.4	37.9 ± 0.1	9.7
16	Luteolin	8.4 ± 0.4	8.2 ± 0.2	1.0

[a] Determined fluorometrically using 1,N^6-etheno NAD^+ as substrate. The values represent means ± SD of three independent experiments.
[b] Selectivity is given by the ratio $IC_{50}^{CD38}/IC_{50}^{SmNACE}$ which were determined at the same $[S]/K_m$ ratio for both enzymes.

about one order of magnitude in favor of *Sm*NACE. Importantly, this result indicates that the molecular requirements providing a binding affinity and selectivity to the active site of *Sm*NACE are reachable. Such an observation is in agreement with known structural specificities of the active site of the parasitic enzyme.[4,8] Finally, the results obtained here might also be of great importance for the design of innovative CD38 inhibitors, a promising therapeutic field handicapped by the paucity of active molecules. The full study on human CD38 inhibition will be reported in due time (I. Kuhn et al., to be published).

3. Discussion

*Sm*NACE, a key enzyme which was recently identified in *S. mansoni*, is one of the rare biochemically characterized protein present at the surface of this parasite.[4] A consensus exists that such surface proteins are privileged targets for the design of therapeutic agents and vaccines. Our present work aimed at finding inhibitors in order to validate this enzyme as a therapeutic target and to eventually design new drugs to fight schistosomiasis.

The predominant activity of the human homologous enzyme CD38 is the hydrolytic cleavage of NAD^+ (NAD^+glycohydrolase activity), but CD38 also catalyzes the conversion of $NAD(P)^+$ to Ca^{2+}-mobilizing messengers such as cyclic ADP-ribose (ADP-ribosyl cyclase activity)[33] and $NAADP^+$.[34] In sharp contrast, the parasitic ecto-*Sm*NACE is basically a NAD^+glycohydrolase that is unable to produce cyclic ADP-ribose.[4] Structural studies based on sequence alignments, homology modeling and site-directed mutagenesis[8] have ascribed this lack of ADP-ribosyl cyclase activity to the occurrence in the active site of *Sm*NACE of a His residue (His103) in replacement of the catalytically important Trp which is strictly conserved in all the other members of this enzyme super-family. These findings, in addition to the observation that some inhibitors have a differential activity against *Sm*NACE and human CD38,[8] support the possibility of discovering specific *Sm*NACE ligands.

Because of the paucity of druggable small-molecule CD38 inhibitors and based on the assumption that enzymes sharing an identical substrate and analogous catalytic mechanisms can be inhibited by similar ligands, we first tested representative inhibitors of NAD^+-utilizing enzymes, such as sirtuins and PARPs, for their ability to block *Sm*NACE activity. But this approach did not prove successful and this failure could be partly explained by structural considerations. NAD^+ is a highly flexible molecule which can adopt various active conformations. In addition, as underlined in this study, the active site of *Sm*NACE does not resemble to any other known NAD^+-binding sites, except that of its distant homolog CD38.

The high-throughput screening of academic libraries (14,300-entries) revealed that despite the great number of chemically diverse compounds tested, only two anthocyanidins, cyanidin (**1**) and delphinidin (**2**), were found that inhibited *Sm*NACE in the

low micromolar range. Many primary HTS hits revealed to be false-positives either because they were aggregators and sensitive to detergent or, when purified, they failed to reiterate their original activity. These factors are unfortunately common pitfalls of HTS, see for example, Ref. 35.

Cyanidin with IC_{50} = 2.3 μM, was a confirmed hit worthy of structure–activity relationship follow-up studies (for the sake of comparison, the K_m value of NAD^+ is 38.5 μM).[4] We investigated the inhibitory potency of structurally related anthocyanidins (**3**–**10**), anthocyanin (**11**) and other flavonoid subgroups such as flavonols (**12**–**15**), flavone (**16**), flavanonol (**17**) and flavan-3-ol (**18**) and *trans*-stilbenoids (**19**, **20**). It appears that almost all flavonoids tested are low micromolar inhibitors of *Sm*NACE. The observed IC_{50} values range from 1.3 μM for quercetagetin to 37.8 μM for petunidin, and depend on the substitution by hydroxyl- or methoxy-groups of the flavonoid scaffold. The only exception being catechin (**18**) which, although sharing large structural similarities with the other flavonoids, failed to inhibit *Sm*NACE activity at 100 μM concentration. Consequently, the geometry of the ring C, which determines the relative positions of ring A and B in space, most probably impacts the flavonoids inhibitory activity. In anthocyanidins and most other flavonoids, ring C is planar, while ring puckering occurs in flavan-3-ols. Our docking studies support this assumption and suggest that anthocyanidins and flavonols/flavones can mimic the nicotinamide-ribosyl moiety of the substrate NAD^+, with efficient H-bonding to residue Glu202. A similar surprising observation was made recently in the interaction of flavonoids with *Helicobacter pylori* β-hydroxyacyl-acyl carrier protein dehydratase. Thus, in contrast to otherwise structurally similar flavonoids such as quercetin, *rac*-naringenin which is lacking the C2–C3 double bond in ring C was totally inactive against this enzyme; this result was also ascribed to the lack of planarity of this flavanone.[36]

The two tested *trans*-stilbenoids **19** and **20**, that is, molecules which have been found active on several enzymes,[37] did not inhibit *Sm*NACE activity. In these compounds, ring C is replaced by an ethylene group, leading to an increased molecular flexibility resulting in an apparent lack of optimal binding.

In cyanidin, and more generally in anthocyanidins, ring C which is positively charged could mimic the oxocarbenium ion-like transition state of the reaction catalyzed by *Sm*NACE.[29] Such analogy, on which the design of many potent glycosidase inhibitors has been based, was particularly appealing. However, the presence of such a positive charge proved not to be mandatory for *Sm*NACE inhibition, since the most potent inhibitor we have discovered, namely quercetagetin (**15**), belongs to the flavone series and is lacking this feature.

The structure–activity relationship indicates that the potency of flavonoids depends on the number and the position of hydroxyl substituents. Strikingly, the best inhibitor of the anthocyanidin series has not the same substitution pattern than the best inhibitor of the other flavonoid series. In light of this complexity, our docking studies gave several clues about ligand-*Sm*NACE recognition, but can not predict the relative affinity of the inhibitors for the active site of this enzyme. The binding properties of the flavonoids is actually not only determined by the set of chemical groups required for intermolecular interaction with the target (i.e., the pharmacophore for *Sm*NACE inhibition), but also by their solubility, hydration and reactivity. At this point, although rarely taken into consideration in publications related to the biological/enzymatic effects of anthocyanidins, the chemical reactivity of these compounds must be discussed. The flavylium cation of anthocyanidins is notoriously unstable in water at neutral pHs.[38] In a series of reversible reactions this oxocarbenium ion undergoes a hydration reaction on the electrophilic 2-position resulting in two epimeric hemiacetals whose hydroxyl groups (e.g., at positions 4′ and 7 in cyanidin) can deprotonate resulting in a rapid equilibrium with tautomeric forms of quinoidal anhydrobases (Fig. 6A). More slowly, and accentuated at higher pH values, C-ring opening and isomerization reactions are also observed yielding the corresponding C_Z- and C_E-chalcones. The rates and equilibrium constants of these interconversion reactions are somewhat dependent on structural parameters,[39] that is, hydroxyl- and methoxyl-substituent patterns and occurrence of glycosylated substituents (anthocyanins), and also on the microenvironment. Related to this latter point the planar flavylium ion can be stabilized by specific interactions, such as π–π stacking, known as intermolecular co-pigmentation reactions. Altogether, when dissolved in water, anthocyanidins are expected to give rise to a mixture of interconverting compounds. At thermodynamic equilibrium, under slightly acidic to neutral conditions, anthocyani(di)ns occur predominantly as hemiacetals.[40] These various molecular species might have different affinities for the active site of the enzyme. Interestingly, however, as observed in the co-pigmentation phenomena[39] hydrophobic interactions within the active site of the enzyme might also displace the overall equilibrium towards a stabilized form of the flavylium cation which is shielded against the nucleophilic attack from water. The docking of all molecular entities deriving from cyanidin into the active site of *Sm*NACE (Figs. 5B and 6B–E) strongly suggests that: (i) the B-ring always fills the site involved in the recognition of the substrate's N-ribose moiety at the bottom of the protein pocket, (ii) a hydroxyl substituent at position 3, 7 or 10 depending of the cyanidin derivative, is H-bonded to the invariant Glu124 carboxylate (the "signature" Glu present in all the active sites of the CD38 super-family), and (iii) ring A and/or C is stacked against Trp165 side-chain. The total count of intermolecular H-bonds suggests a preference of *Sm*NACE for the 2*R*-configuration of the hemiacetal, which can establish additional H-bonds with Thr197, Ser169 and His162.

In reason of the low rate of success of our HTS campaign, *Sm*NACE can be categorized into the 'difficult' class of targets. In addition, the peculiar three-dimensional architecture of the active site of this enzyme largely restricts the source of inspiration for the rational design of inhibitors. The identified competitive *Sm*NACE inhibitors although active in the micromolar range are valuable hits for the several reasons. First, flavonoids are small polar and water-soluble compounds. They are well suited tools for the validation of *Sm*NACE as drug target to fight schistosomiasis. Second, though flavonoids are promiscuous ligands that bind to number of enzymes and receptors[41–43] and are thus poorly druggable, they have good ligand efficiency (i.e., affinity reported to the number of non-hydrogen atoms) ranging from 0.23 to 0.38 kcal/mol and provide worthwhile information for drug design. The SAR data pointed out the interaction requirements and gave clues for the design of a three-dimensional pharmacophore. Last, relatively simple chemical modifications of flavonoids would allow the investigation of the selectivity issue. There exist structural differences between *Sm*NACE and its human homolog CD38 suggesting that it is possible to improve the inhibitor selectivity by rational optimization. More precisely, the bottom of the enzyme active site cavity is larger in *Sm*NACE than in human CD38, because of the tryptophan to histidine (His103) replacement, moreover the amino acid composition of the active site mouth differs in the parasite and mammalian enzymes.

In conclusion, we have identified 17 natural compounds which inhibit *Sm*NACE with IC_{50} values in the micromolar range, the most potent being quercetagetin and cyanidin. This novel class of inhibitors will be helpful to unravel the biological role of *Sm*NACE and further investigations are now necessary to investigate the potential of this enzyme as a drug target for schistosomicidal activity.

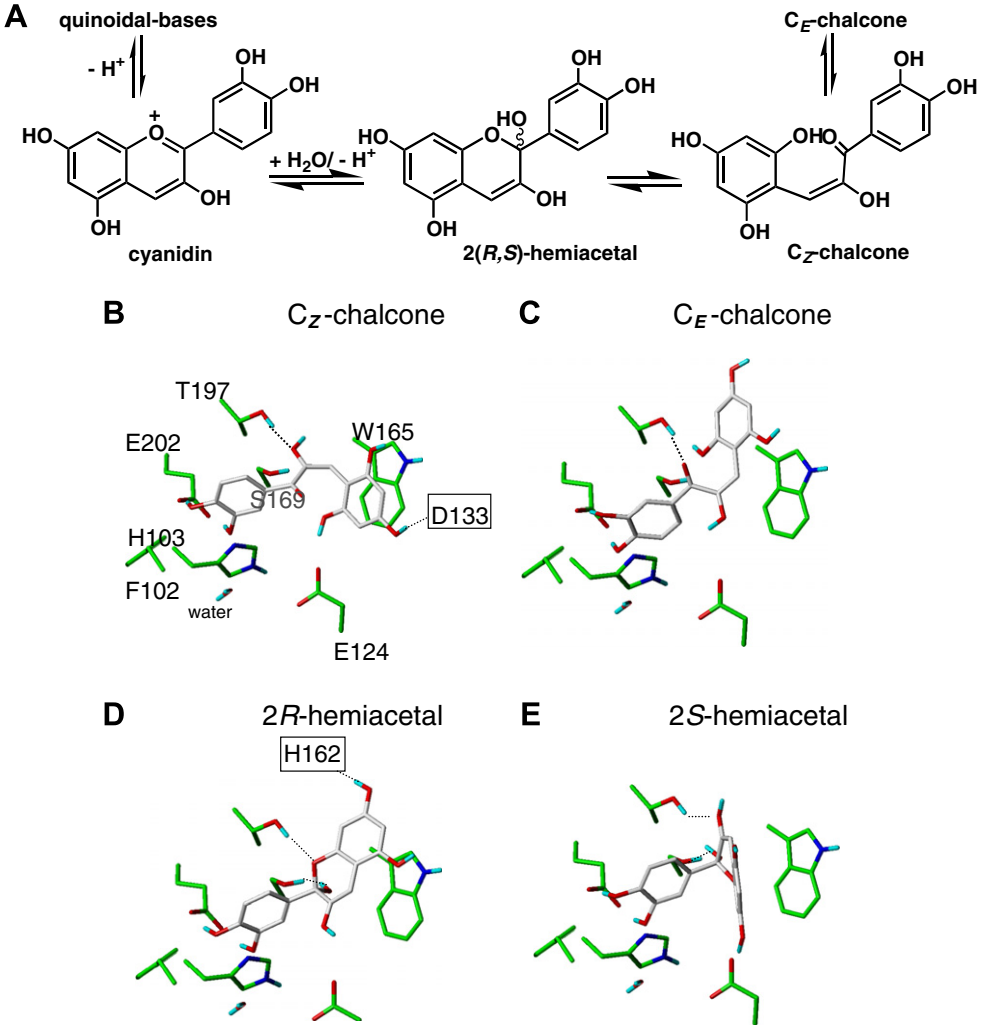

Figure 6. Molecular species derived from cyanidin docked into the active site of *Sm*NACE. (A) Simplified scheme for the structural transformation of cyanidin in aqueous media. The C_Z-chalcone (B), C_E-chalcone (C), 2*R*-hemiacetal (D) and 2*S*-hemiacetal (E) derivatives of cyanidin docked into *Sm*NACE. The protein binding sites are represented by the side-chain of key active site catalytic residues and are displayed, as the ligands, as capped sticks. The color coding is similar to Figure 5. Carbon, grey and green for cyanidin derivatives and *Sm*NACE, respectively. The H-bonds with Thr197, Ser169 and His162 are highlighted with dotted lines.

4. Experimental

4.1. Reagents

NAD^+, 1,N^6-etheno NAD^+, Cibacron blue 3GA, curcumin, suramin and PJ-34 were purchased from Sigma–Aldrich (St. Quentin Fallavier, France). Acetophenone (99% extra pure) was purchased from Acros Organics (Noisy-le-Grand, France). Formic acid and potassium hydroxide were from Riedel-de Haën (Sigma–Aldrich). Anthocyanidins, anthocyanins and flavonoids were purchased from Extrasynthese (purity ranging from 95% to 99%) (Genay, France). The 96-well fluorescence plates (half-area, black, non-binding surface) were purchased from Corning (Cergy, France).

4.2. Expression and purification of *Sm*NACE and human CD38

Recombinant *Sm*NACE was expressed in *Pichia pastoris* and purified on a Blue Sepharose 6 fast flow CL-6B column as previously described.[4] The human CD38 cDNA clone in pCDNA-3 was a kind gift of Dr. P. Deterre (Laboratoire d'Immunologie Cellulaire, Groupe Hospitalier Pitié-Salpêtrière, Paris). Restrictions sites were introduced by PCR, respectively NotI at nucleotide 205, leading to the deletion of 45 residues in the N-terminal domain of the protein encompassing its intracellular and membrane spanning regions, and XbaI at position 1011 conserving the stop codon. The primers used were designed as follows: forward, 5′-AAA-TAT**GCGGCCGC**TGGCGCCAGCAGTGGAGCGGTCCG-3′ and reverse, 5′-TGC**TCTAGA**CAAGGAGCTAGGGAGCTAAA-3′ (the restriction sites are in bold). To produce CD38 in *P. pastoris*, the sequence was subcloned into the expression vector pPICZαA (Invitrogen). Recombinant CD38-pPICZαA plasmid containing the insert was sequenced to ensure its sequence integrity. A soluble recombinant form of the ecto-domain of human CD38 containing its four N-glycosylation sites (wild-type) was expressed as a secreted protein and affinity-purified as previously described for bovine CD38.[44]

4.3. Kinetic measurements

*Sm*NACE activity was determined by a continuous fluorometric method using ε-NAD^+ as substrate, as previously described.[21] This assay consists in measuring the appearance of the reaction product ε-ADP-ribose by the increase of fluorescence at λ_{em} = 410 nm (λ_{exc} = 310 nm) at 37 °C in 10 mM potassium phosphate buffer, pH 7.4, containing 0.05% (w/v) emulphogen (1 mL final volume) in a thermostatically controlled fluorimeter cuvette (Shimadzu, RF 5301 PC). Alternatively, the activity was measured at 20 μM

NAD^+ as previously described,[4] by following the product formation by HPLC on a 300 × 3.9 mm μBondapack C_{18} column (Waters). The isocratic elution was performed at a flow rate of 1 mL/min (10 mM ammonium phosphate buffer, pH 5.5, with 1.2% (v/v) acetonitrile), and monitored by absorbance at 260 nm.

The effect of the inhibitors on the initial rates of the transformation of 20 μM ε-NAD^+, that is, at a [S]/K_m ratio equal to 0.88, were determined and IC_{50} values were calculated from the plot of residual activity against the log of inhibitor concentration (8 data points, in triplicate) using a non-linear regression program (GrapPad, Prism). The IC_{50} obtained by the fluorometric assay were systematically validated by control experiments using the HPLC assay run in the presence of [I] = IC_{50}. The type of inhibition was determined under the same experimental conditions using four different fixed inhibitor concentrations and varying ε-NAD^+ concentrations. The kinetic parameters were calculated, as above, from the data using the classical enzyme kinetic equations.[45]

4.4. High-throughput screening

The compound library used for the high-throughput screening was from the French National Library (http://chimiotheque-nationale.enscm.fr/), it included 4800 synthetic compounds and 480 natural products originating from the UMR 7200 CNRS-University of Strasbourg (Illkirch, France) and 8100 synthetic compounds from the UMR 176 CNRS-Institut Curie (Paris, France). Additionally, a sub-set (880 off-patent FDA-approved drugs) of the Prestwick Chemical Library was also tested. Altogether the screening was performed with a library of about 14,300 molecules characterized by an important chemical diversity[27] that includes heterocyclic molecules, small peptides and amino acid derivatives. It is organized in 96-well plates each containing 80 compounds, dissolved in DMSO to a concentration of 10 mM, leaving 16 empty wells for controls.

Our experimental screening assay is based on the *Sm*NACE catalyzed hydrolysis of NAD^+ to nicotinamide and ADP-ribose, followed by a chemical conversion of the residual substrate into a fluorescent compound. For each assay the compounds to be tested were first serially diluted to 50 μM in 10 mM potassium phosphate, pH 7.4, DMSO 0.5%.v/v (parent plate) and transferred to duplicate plates at 5 μL per well. β-NAD^+ was then added at 10 μM final concentration in 10 mM potassium phosphate, pH 7.4, DMSO 0.1% v/v and the enzymatic reaction was initiated by the addition of 50 ng *Sm*NACE (specific activity: 5.5 μmol/min/mg protein). Positive and negative control wells in the first and last rows, contained NAD^+ and DMSO 0.1% v/v, with or without enzyme. In addition, on each plate 3 wells to which 100 μM of the inhibitor Cibacron blue 3GA[8] was added were used as positive inhibition controls. The final reaction volume in each well was 25 μL. After 10 min of incubation at room temperature, 10 μL of 2 M aqueous KOH solution and 10 μL of a 20% acetophenone/80% ethanol mixture were added per well. The plate was then incubated at 4 °C for 10 min. After addition of 45 μL of 88% formic acid, the plate was incubated at 110 °C for 5 min (final volume: 90 μL/well). Dilution and mixing of all components was carried out on a fully automated Beckman Coulter robotized platform (PCBIS). After cooling, the fluorescence was recorded using a microplate reader Victor (Perkin Elmer) with 355 nm and 460 nm as excitation and emission wavelengths, respectively. The stability of the measured fluorescence was tested as a function of time and no significant change was observed for 30 min. For each plate, the control wells with NAD^+ in the presence or absence of *Sm*NACE were used to calculate the *Z′*-factor, a statistical coefficient integrating parameters such as the signal-to-noise ratio and data dispersion, which reflects the quality of the assay.[26]

The hit threshold was set at >40% of reaction inhibition, that is, fluorescence decrease (% of inhibition = 100* (mean of positive control − hit value)/(mean of positive control − mean of negative control). To detect the fluorescence that might be inherent to the compounds under evaluation, wells containing only the diluted compounds (at 20 μM) were measured independently. The value of any intrinsic fluorescence detected in the compounds was subtracted. Confirmation of the primary hits was performed in duplicate at 1 μM and 10 μM final concentrations using cherry picked compounds. The hit threshold was set at >40% inhibition for this second screen. All experiments were performed according quality management control (ISO 9001).

4.5. Hit validation

To validate the initial hits and eliminate the false-positives—such as promiscuous aggregate-based inhibitors—which are inherent to the HTS methodology, secondary screens were performed. Inhibition of *Sm*NACE was investigated in greater detail by performing individual assays with compounds which originated from the original compound stock and obtained, when available, in an analytically pure form. IC_{50} values were determined with a low-throughput procedure using the same assay as for HTS (see above), but varying the concentration of the tested compounds (in triplicate). The final fluorescence was measured using a SpectraMax Gemini XPS microplate reader (Molecular Devices, Sunnyvale, CA) at λ_{em} = 460 nm (λ_{exc} = 355 nm) and a SoftMax Pro software. Finally, for the most promising compounds, dose–response curves were established with the fluorometric assay using ε-NAD^+ as substrate (See Section 4.3). To eliminate the potential aggregators the assays were performed in the presence of 0.1% Triton X-100.

4.6. Modeling of *Sm*NACE active site and docking

The overall three-dimensional structure of *Sm*NACE has been previously modeled by homology to human CD38 (the sequence identity between the two enzymes is 24%).[4,8] It was updated by integrating additional templates (recent crystal structures of human holo-CD38 and in-house structures of bovine CD38 (to be published)). The active site of *Sm*NACE is located at the bottom of a pocket made by the 15 following residues: Tyr101, Phe102, His103, Ser104, Arg111, Ser122, Leu123, Glu124, Asp133, Trp165, Ser169, Tyr172, Thr197, Phe198 and Glu202. The *Sm*NACE binding site was compared to the 7070 druggable protein binding sites extracted from PDB entries (sc-PDB database, 2009 release).[30] The similarity was evaluated on aligned three-dimensional structures using SITEALIGN4.0 program.[31] Hits are selected if the D1 distance is lower than 0.6, the D2 distance is lower than 0.2, and the RMSD between atoms of overlaid sidechains is below 3 Å.

The three-dimensional structures of compounds **1**–**17** were sketched and energy minimized using SybylX.0 (Tripos Inc., Saint Louis, USA), then docked into *Sm*NACE binding site using GOLD v4.1 (CCDC, Cambridge, UK). The protein binding site was defined using the above defined list of residues. A water molecule was built in the bottom of the pocket, to mimic the water molecule bridging Leu145 and Leu123 backbone atoms in all available human and bovine CD38 crystal structures. Docking of flavonoids **1**–**17** into *Sm*NACE was also carried out using SURFLEX v2.412 (Tripos Inc., Saint Louis, USA). The promotol generation and the docking were performed using the default settings. The number of output poses was set to 10.

Acknowledgments

This work was supported financially by the CNRS, the French Ministry of Research and the Agence Nationale de la Recherche

(Grant ANR-05-BLAN-0076 to F.S. and D.R.). We are grateful to David S. Grierson, Jean-Claude Florent and Florence Mahuteau-Betzer for providing the Chemical library of UMR 176 CNRS-Institut Curie (Paris, France) and for discussions. We thank Bruno Didier for the locally sourced products. The technical expertise of Adeline Obrecht and Christel Husser (PCBIS-Illkirch) is acknowledged. F.S., H.M.-S., and E.K. designed and supervised the study. H.M.-S. developed the *Sm*NACE fluorometric activity assay for high-throughput screening and P.V. was involved in its optimization. P.V. supervised the HTS of the compound libraries and carried out the statistical analysis. E.K. performed the bio- and cheminformatic studies. F.S.-H., H.M.-S. and I.K. made all the other reported experiments. F.S., H.M.-S. and E.K. wrote the paper.

Supplementary data

Supplementary data (Table S1, Figs. S1–S5) associated with this article can be found, in the online version, at doi:10.1016/j.bmc.2010.09.041.

References and notes

1. Doenhoff, M. J.; Hagan, P.; Cioli, D.; Southgate, V.; Pica-Mattoccia, L.; Botros, S.; Coles, G.; Tchuente, L. A. T.; Mbaye, A.; Engels, D. *Parasitology* **2009**, *136*, 1825.
2. Caldas, I. R.; Campi-Azevedo, A. C.; Oliveira, L. F.; Silveira, A. M.; Oliveira, R. C.; Gazzinelli, G. *Acta Trop.* **2008**, *108*, 109.
3. Layland, L. E.; Mages, J.; Loddenkemper, C.; Hoerauf, A.; Wagner, H.; Lang, R.; da Costa, C. U. *J. Immunol.* **2010**, *184*, 713.
4. Goodrich, S. P.; Muller-Steffner, H.; Osman, A.; Moutin, M. J.; Kusser, K.; Roberts, A.; Woodland, D. L.; Randall, T. D.; Kellenberger, E.; LoVerde, P. T.; Schuber, F.; Lund, F. E. *Biochemistry* **2005**, *44*, 11082.
5. Scheuplein, F.; Schwarz, N.; Adriouch, S.; Krebs, C.; Bannas, P.; Rissiek, B.; Seman, M.; Haag, F.; Koch-Nolte, F. *J. Immunol.* **2009**, *182*, 2898.
6. Lee, H. C. *Annu. Rev. Pharmacol. Toxicol.* **2001**, *41*, 317.
7. Lund, F. E. *Mol. Med.* **2006**, *12*, 328.
8. Kuhn, I.; Kellenberger, E.; Rognan, D.; Lund, F. E.; Muller-Steffner, H.; Schuber, F. *Biochemistry* **2006**, *45*, 11867.
9. Sauve, A. A.; Schramm, V. L. *Biochemistry* **2002**, *41*, 8455.
10. Slama, J. T.; Simmons, A. M. *Biochemistry* **1989**, *28*, 7688.
11. Cen, Y. *Biochim. Biophys. Acta* **2010**, *1804*, 1635.
12. Jagtap, P.; Szabo, C. *Nat. Rev. Drug Disc.* **2005**, *4*, 421.
13. Agrawal, D. K.; Mishra, P. K. *Med. Res. Rev.* **2010**, *30*, 818.
14. Magalhaes, L. G.; Machado, C. B.; Morais, E. R.; Moreira, E. B.; Soares, C. S.; da Silva, S. H.; Da Silva Filho, A. A.; Rodrigues, V. *Parasitol. Res.* **2009**, *104*, 1197.
15. Xiao, S. H.; Chollet, J.; Utzinger, J.; Mei, J. Y.; Jiao, P. Y.; Keiser, J.; Tanner, M. *Parasitol. Res.* **2009**, *105*, 853.
16. Yates, S. P.; Taylor, P. L.; Jorgensen, R.; Ferraris, D.; Zhang, J.; Andersen, G. R.; Merrill, A. R. *Biochem. J.* **2005**, *385*, 667.
17. Lehtio, L.; Jemth, A. S.; Collins, R.; Loseva, O.; Johansson, A.; Markova, N.; Hammarstrom, M.; Flores, A.; Holmberg-Schiavone, L.; Weigelt, J.; Helleday, T.; Schuler, H.; Karlberg, T. *J. Med. Chem.* **2009**, *52*, 3108.
18. Schuetz, A.; Min, J.; Antoshenko, T.; Wang, C. L.; Allali-Hassani, A.; Dong, A.; Loppnau, P.; Vedadi, M.; Bochkarev, A.; Sternglanz, R.; Plotnikov, A. N. *Structure* **2007**, *15*, 377.
19. Turgeon, Z.; White, D.; Jorgensen, R.; Visschedyk, D.; Fieldhouse, R. J.; Mangroo, D.; Merrill, A. R. *FEMS Microbiol. Lett.* **2009**, *300*, 97.
20. Graeff, R.; Lee, H. C. *Biochem. J.* **2002**, *367*, 163.
21. Muller, H. M.; Muller, C. D.; Schuber, F. *Biochem. J.* **1983**, *212*, 459.
22. Nakamura, H.; Tamura, Z. *Anal. Chem.* **1978**, *50*, 2047.
23. Putt, K. S.; Hergenrother, P. J. *Anal. Biochem.* **2004**, *326*, 78.
24. Feng, Y.; Wu, J.; Chen, L.; Luo, C.; Shen, X.; Chen, K.; Jiang, H.; Liu, D. *Anal. Biochem.* **2009**, *395*, 205.
25. Wu, G.; Yuan, Y.; Hodge, C. N. *J. Biomol. Screen.* **2003**, *8*, 694.
26. Zhang, J. H.; Chung, T. D.; Oldenburg, K. R. *J. Biomol. Screen.* **1999**, *4*, 67.
27. Krier, M.; Bret, G.; Rognan, D. *J. Chem. Inf. Model.* **2006**, *46*, 512.
28. Shoichet, B. K. *Drug Discovery Today* **2006**, *11*, 607.
29. Schuber, F.; Lund, F. E. *Curr. Mol. Med.* **2004**, *4*, 249.
30. Kellenberger, E.; Muller, P.; Schalon, C.; Bret, G.; Foata, N.; Rognan, D. *J. Chem. Inf. Model.* **2006**, *46*, 717.
31. Schalon, C.; Surgand, J. S.; Kellenberger, E.; Rognan, D. *Proteins* **2008**, *71*, 1755.
32. Liu, Q.; Kriksunov, I. A.; Graeff, R.; Munshi, C.; Lee, H. C.; Hao, Q. *J. Biol. Chem.* **2006**, *281*, 32861.
33. Lee, H. C. *Mol. Cell. Biochem.* **1994**, *138*, 229.
34. Aarhus, R.; Graeff, R. M.; Dickey, D. M.; Walseth, T. F.; Lee, H. C. *J. Biol. Chem.* **1995**, *270*, 30327.
35. Posner, B. A.; Xi, H.; Mills, J. E. *J. Chem. Inf. Model.* **2009**, *49*, 2202.
36. Zhang, L.; Kong, Y.; Wu, D.; Zhang, H.; Wu, J.; Chen, J.; Ding, J.; Hu, L.; Jiang, H.; Shen, X. *Protein Sci.* **2008**, *17*, 1971.
37. Beckmann, S.; Buro, C.; Dissous, C.; Hirzmann, J.; Grevelding, C. G. *PLoS Pathog.* **2010**, *6*, e1000769.
38. Brouillard, R.; Delaporte, B. *J. Am. Chem. Soc.* **1977**, *99*, 8461.
39. Elhabiri, M.; Figueiredo, P.; Saito, N.; Brouillard, R. *J. Chem. Soc., Perkin Trans. 2* **1997**, 355.
40. Pina, F. *J. Chem. Soc., Faraday Trans.* **1998**, *94*, 2109.
41. Holder, S.; Lilly, M.; Brown, M. L. *Bioorg. Med. Chem.* **2007**, *15*, 6463.
42. Adisakwattana, S.; Charoenlertkul, P.; Yibchok-Anun, S. *J. Enzyme Inhib. Med. Chem.* **2009**, *24*, 65.
43. Williams, C. A.; Grayer, R. J. *Nat. Prod. Rep.* **2004**, *21*, 539.
44. Muller-Steffner, H.; Kuhn, I.; Argentini, M.; Schuber, F. *Protein Expr. Purif.* **2010**, *70*, 151.
45. Copeland, R. A. *Evaluation of Enzyme Inhibitors in Drug Discovery*; John Wiley & Sons: Hoboken, New Jersey, 2005.